Do Small Cells Make Sense for Simple Low Cost LPWANs?

Ashwin Natraj Arun, Anindya Bijoy Das, *Member, IEEE*, Christopher G. Brinton, David J. Love, *Fellow, IEEE*, and James V. Krogmeier

***Abstract*—The increasing adoption of low power wide area networks (LPWANs) for Internet of Things (IoT) devices requires a thorough examination of network dynamics for multi-cell networks. This letter introduces a novel scheme for multi-cell LPWAN and assesses the success probability for end devices at the cell edge using stochastic geometry to model intra-cell interference. We identify the optimal number of cells for a guaranteed minimum success probability, revealing that small cells enhance the average signal-to-interference-noise ratio. It benefits devices at the cell edge, addressing the challenges posed by the growing number of IoT devices in LPWANs.**

***Index Terms*—LPWAN, IoT, long range (LoRa), stochastic geometry.**

I. Introduction

IN RECENT years, the widespread adoption of Internet of Things (IoT) devices has led to a surge in the popularity of wireless sensor networks (WSN). These IoT devices are often small, battery-operated, and used for handling the intermittent traffic. The rapid growth of IoT devices [1] finds applications across diverse domains such as precision agriculture, Industrial IoT (IIoT) and Smart Cities, fundamentally transforming daily life [2]. In agriculture, the strategic placement of IoT sensors has proven to be a game-changer, contributing to an impressive increase of at least 20% in the net annual income for farmers [3]. Currently, the average deployment on farms is 2–3 sensors per acre, a relatively low number [4]. This number is expected to grow exponentially in the future due to the decreasing costs associated with IoT sensor technologies.

To enable efficient communication for these sensors, low power wide area network (LPWAN) technologies are crucial [5]. Notable commercially available LPWAN technologies include SigFox, LoRaWAN and NarrowBand-IoT (NB-IoT). LoRaWAN [6] utilizes Long Range (LoRa) with chirp spread spectrum for extended sub-GHz industrial, scientific, medical (ISM) band communication, achieving low power and a range of up to 10-20 km in line-of-sight channels. SigFox [7] employs ultra-narrow band modulation for low-power, long-range communication. NB-IoT [8], following 3GPP standards, operates under LTE and 5G-NR networks, providing long-range communication. NB-IoT and SigFox use narrowband for uplink transmissions, while LoRa employs chirp spread spectrum with quasi-orthogonal codes for multiple access.

Manuscript received 6 April 2024; revised 24 May 2024; accepted 3 June 2024. Date of publication 7 June 2024; date of current version 11 September 2024. This work was supported in part by the National Science Foundation under Grant EEC-1941529, Grant CNS-2212565, and Grant CNS-2235134. The associate editor coordinating the review of this article and approving it for publication was G. Chen. *(Corresponding author: Ashwin Natraj Arun.)*

The authors are with the School of Electrical and Computer Engineering, Purdue University, West Lafayette, IN 47907 USA (e-mail: ashwin97@purdue.edu; das207@purdue.edu; cgb@purdue.edu; djlove@purdue.edu; jvk@purdue.edu).

Digital Object Identifier 10.1109/LWC.2024.3411470

In [9], [10], [11], the authors have examined uplink transmission in multi-cell LoRa systems, assuming clustered end devices (EDs) around gateways (GWs). Despite LoRa's simplicity, inter-cell interference grows with cell count, highlighting the need for a simple, inter-cell interference-free LPWAN. To the best of our knowledge, there is no prior work on mitigating inter-cell interference in LPWANs. Our work addresses this gap by proposing a communication scheme for LPWANs and determining the optimal number of cells for a guaranteed minimum success probability.

Specifically, we explore the effectiveness of small cells in LPWANs using orthogonal frequency separation. In each cell, all the EDs within the cell transmit data to the GW at the center of the cell. To address the inter-cell interference, we propose a novel scheme that allocates orthogonal frequency channels to each individual cell. The orthogonality of the channels ensures that only the EDs within a cell transmit on the same channel, effectively eliminating inter-cell interference. To model the intra-cell interference from other EDs in a multi-cell LPWAN, we employ stochastic geometry [12]. Our metric for evaluation is the success probability at the cell edge, for which we derive closed-form expressions. Using it, we determine the optimal number of cells required for effective LPWAN coverage over a large area, guaranteeing a minimum success probability. Our contributions in this letter are summarized below.

- We introduce a multiple access scheme and network deployment based orthogonal frequency allocation in simple cells. Our proposed scheme helps to mitigate inter-cell interference, addressing the deficiency of multi-cell LoRa.
- We model the intra-cell interference from concurrent EDs in a cell using stochastic geometry. This aids in computing the success probability of an uplink transmission from an ED at the cell-edge to the GW. We compute the optimal number of cells that guarantees a minimum success probability with our proposed scheme that facilitates network deployment.
- We conduct simulations to verify our analytical results on the success probability and optimal number of cells. Also, we demonstrate the performance improvements of our scheme relative to multi-cell LoRa [9].

II. System Model

In this section, we model the uplink communication between an ED at the cell boundary and its serving GW in a multi-cell LPWAN. We focus on the uplink transmission between the EDs and the GW, as uplink communication is more constrained in an LPWAN.

A. Spatial Model

We consider a multi-cell LPWAN that covers a square region $\mathcal{F}$ with side length d and area $A = d^2$. The region $\mathcal{F}$

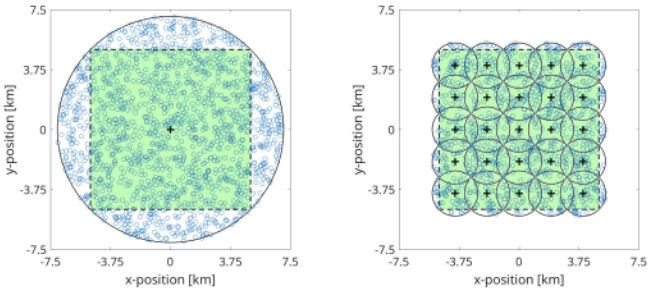

Fig. 1. We consider an N-cell LPWAN covering the region $\mathcal{F}$ (green square). We cover $\mathcal{F}$ with N overlapping cells where the radius of each small cell is $d/\sqrt{2N}$. Each cell has its own orthogonal frequency channel and a GW at the center of the cell. A few realizations of EDs and the GWs in a multi-cell LPWAN is shown. Here the gateways are located at the markers + and the EDs are at the markers o for an area $A = 100\text{km}^2$.

is covered with small overlapping circular cells, each with a radius $R = d/\sqrt{2N}$, where N is the number of cells. Each cell has a GW located at its center. The spacing between GWs in both the x and y directions is $d/\sqrt{N}$, ensuring that every point in $\mathcal{F}$ is covered by at least one cell. A few configurations of this setup are illustrated in Fig. 1. In our scheme, each small cell is allocated an orthogonal frequency channel, and all the EDs within the cell communicate with the GW at the center of the cell via the allocated channel. The total allocated bandwidth for the LPWAN is denoted as W, with the fractional bandwidth assigned to each small cell being $B = W/N$. All the EDs within a cell independently transmit signals to the corresponding GW. Since each cell has a unique non-overlapping frequency channel, there is no inter-cell interference between the EDs. Unlike LoRa, in our scheme, an ED communicates with only one GW rather than multiple GWs. We model the location of EDs using a homogeneous Poisson point process (HPPP) Φ_{ED} with density λ_{ED}. ALOHA with capture effect [13] serves as our medium access control (MAC) protocol, where the probability that an ED transmits a packet is p. Due to the thinning property in HPPP [12], the location of active EDs also form an HPPP Φ_{AED} with density $\lambda_{AED} = p\lambda_{ED}$. Therefore, the average number of active EDs in a cell is denoted as $\bar{L}_N = p\lambda_{ED}\frac{\pi d^2}{2N}$.

B. Signal and Channel Model

In our analysis of the uplink communication channel, we focus on the worst-case scenario, where the desired ED is positioned at the cell edge, and the GW is located at the cell center. We also assume that all the EDs in the overlapping regions within the cell communicate with the corresponding GW at the center of the cell, as this accounts for maximal interference. The communication occurs through an orthogonal frequency channel, where all EDs within the cell transmit on the same channel with a bandwidth B and a carrier frequency f_c. Each ED is equipped with an omni-directional antenna and transmits with power P. The distance between the desired ED and the GW is the radius of the cell, $R = d/\sqrt{2N}$. The channel model incorporates both small-scale fading and large-scale effects characterized by a pathloss function $\ell(\cdot)$. Additive white Gaussian noise (AWGN) is also considered in the model, with zero mean and noise variance $\sigma^2 = N_0 B$, where N_0 is the AWGN power spectral density. The transmit signal-to-noise ratio (SNR) of the ED is denoted as $\rho = P/\sigma^2$. The received signal y at the GW is modeled as

$$y = \sqrt{\rho\ell(R)}\, h\, x + \sum_{i\in\Phi_{AED}} \sqrt{\rho\ell(d_i)}\, g_i x_i + w, \qquad (1)$$

where h is the fading coefficient between the ED and the GW, g_i is the fading coefficient between the i^{th} interfering ED and the GW, and $w \sim \mathcal{CN}(0,1)$ represents the AWGN affecting the transmitted signal. In case of Rayleigh block fading, both h and g_i are independent and identically distributed (i.i.d.) complex Gaussian random variables with zero mean and unit variance. The distance of the i^{th} interfering ED from the serving GW is denoted as d_i. Symbols transmitted from the ED and interfering EDs are represented by x and x_i respectively, where $x, x_i \sim \mathcal{CN}(0,1)$. This implies that x and x_i are drawn from a Gaussian codebook to maximize the mutual information. The large-scale pathloss due to distance is denoted by $\ell(d) = \kappa d^{-\alpha}$, where α is the pathloss exponent (in realistic scenarios $\alpha \geq 2$ [11]), $\kappa = (\mu_c/4\pi)^2$ represents the pathloss coefficient due to large-scale fading and μ_c is the wavelength of the carrier signal.

III. Uplink Performance Analysis in a Poisson Field of Interferes

For the signal model presented in Section II-B, the signal-to-interference-plus-noise ratio (SINR) for a signal transmitted by an ED to the corresponding GW in a cell is

$$\text{SINR} = \frac{\rho\ell(R)|h|^2}{\sum_{i\in\Phi_{AED}} \rho\ell(d_i)|g_i|^2 + 1}. \qquad (2)$$

The success probability of transmission from the ED at the cell-edge to the serving GW in an N-cell LPWAN is

$$P_{suc}(N) = \mathbb{P}\left(\frac{W}{N}\log_2(1+\text{SINR}) \geq r\right). \qquad (3)$$

Here, r is the target bit-rate of the LPWAN for proper reception. Let $\mathcal{I}_{cell} = \sum_{i\in\Phi_{AED}} \rho\ell(d_i)|g_i|^2$ be the intra cell interference caused by active EDs transmitting concurrently in the same channel. Then, (3) can be rewritten as

$$P_{suc}(N) = \mathbb{P}(\text{SINR} \geq \theta) = \mathbb{P}\left(\frac{\rho\ell(R)|h|^2}{\mathcal{I}_{cell}+1} \geq \theta\right)$$
$$= \mathbb{P}\left(|h|^2 \geq \frac{\theta(\mathcal{I}_{cell}+1)}{\rho\ell(R)}\right). \qquad (4)$$

where $\theta = 2^{\frac{N_r}{W}} - 1$ is the SINR threshold required for the GW to successfully decode the desired signal from the ED. By conditioning on $\mathcal{I}_{cell}$, (4) is simplified as

$$P_{suc}(N) = \int \mathbb{P}\left(|h|^2 \geq \frac{\theta(y+1)}{\rho\ell(R))}\right) f_{\mathcal{I}_{cell}}(y)\, dy$$
$$= \mathbb{E}_{\mathcal{I}_{cell}}\left[\mathbb{P}\left(|h|^2 \geq \frac{\theta(\mathcal{I}_{cell}+1)}{\rho\ell(R)}\right)\right]. \qquad (5)$$

With Rayleigh fading $F_{|h|^2}(x) = 1 - e^{-x}$, so (5) can be rewritten as

$$P_{suc}(N) = \exp\left(-\frac{\theta}{\rho\ell(R)}\right)\mathbb{E}_{\mathcal{I}_{cell}}\left[\exp\left(-\frac{\theta\mathcal{I}_{cell}}{\rho\ell(R)}\right)\right]. \qquad (6)$$

Using the moment generating function (MGF) $\mathcal{L}_{\mathcal{I}_{cell}}(s)$ of the total interference power $\mathcal{I}_{cell}$ in (6),

$$P_{suc}(N) = \exp\left(-\frac{\theta}{\rho\ell(R)}\right)\mathcal{L}_{\mathcal{I}_{cell}}\left(\frac{\theta}{\rho\ell(R)}\right). \quad (7)$$

Next we state the following lemma (with the proof in Appendix A) which computes the moment generating function of intra-cell interference.

Lemma 1: The MGF of the intra-cell interference $\mathcal{L}_{\mathcal{I}_{cell}}(s)$ can be expressed as

$$\mathcal{L}_{\mathcal{I}_{cell}}(s) = \exp\left(-2\pi p\lambda_{ED}\int_0^R \frac{s\rho\kappa x^{-\alpha}}{1+s\rho\kappa x^{-\alpha}}xdx\right). \quad (8)$$

For $\alpha > 2$, there is no closed form expression for (8). Hence, we use Gauss-Chebyschev quadrature [14] to find an approximation of (8) as

$$\mathcal{L}_{\mathcal{I}_{cell}}(s) \approx \exp\left(-\frac{1}{N}\frac{p\lambda_{ED}(\pi d)^2}{2n}\sum_{k=1}^{n}\frac{c_k\sqrt{1-\psi_k^2}}{1+\frac{c_k^{\alpha}d^{\alpha}}{s\rho\kappa 2^{\frac{\alpha}{2}}N^{\frac{\alpha}{2}}}}\right), \quad (9)$$

where $\psi_k = \cos(\frac{2k-1}{n}\pi)$, $c_k = \frac{\psi_k+1}{2}$ and n is the number of points generated for numerical approximation.

Now, we have $\theta = 2^{\frac{Nr}{W}} - 1$, $\rho = \frac{P}{N_0 B}$ and $\ell(R) = \kappa R^{-\alpha}$, where $R = \frac{d}{\sqrt{2N}}$. Thus, we can say

$$\frac{\theta}{\rho\ell(R)} = \frac{2^{\frac{Nr}{W}}-1}{\frac{P}{N_0 B}\kappa R^{-\alpha}} = \frac{d^{\alpha}\left(2^{NG}-1\right)}{\frac{PN}{N_0 W}\kappa 2^{\frac{\alpha}{2}}N^{\frac{\alpha}{2}}} = \frac{d^{\alpha}N_0 W\left(2^{NG}-1\right)}{P\kappa 2^{\frac{\alpha}{2}}N^{\frac{\alpha}{2}+1}}, \quad (10)$$

where $G = \frac{r}{W}$ and $B = \frac{W}{N}$. The success probability of an ED at the cell-edge as a function of N can be computed from (7) using (9) and (10) as

$$P_{suc}(N) \approx \exp\left(-\frac{F\left(2^{NG}-1\right)}{N^{\frac{\alpha}{2}+1}} - \frac{H}{N}\sum_{k=1}^{n}\frac{c_k\sqrt{1-\psi_k^2}}{1+\frac{c_k^{\alpha}}{2^{NG}-1}}\right) \quad (11)$$

where $F = \frac{d^{\alpha}N_0 W}{P\kappa 2^{\frac{\alpha}{2}}}$, and $H = \frac{p\lambda_{ED}(\pi d)^2}{2n}$.

IV. Optimal Number of Cells

In this section, we compute the optimal number of cells that guarantees a minimum success probability of an ED at the cell edge. Formally, we define the optimal number of cells $N^{\star}$ as the minimum N that satisfies the success probability constraint $P_{suc}(N) \geq \beta$ for a target β. Writing $P_{suc}(N) = e^{f(N)}$, the optimal number of cells $N^{\star}$ can be computed from,

$$N^{\star} = \arg\min_N \; f(N) \quad \text{subject to } f(N) \geq \log(\beta). \quad (12)$$

We list some important properties of $f(N)$ in Lemma 2 (with a detailed proof in Appendix B).

Lemma 2: When N is small, $f(N)$ is an increasing function. On the other hand, when N is large, it is a decreasing function.

Thus, according to Lemma 2, $P_{suc}(N) = e^{f(N)}$ is not simply monotonically increasing with N. While it is an increasing function for small N, it is a decreasing function for large values of N. Now, the optimal number of cells (denoted by $N^{\star}$) can be computed from (12) using an exhaustive search across $f(N)$ with the success probability constraint where $f(N) = \log(P_{suc}(N))$ and can be evaluated using (11).

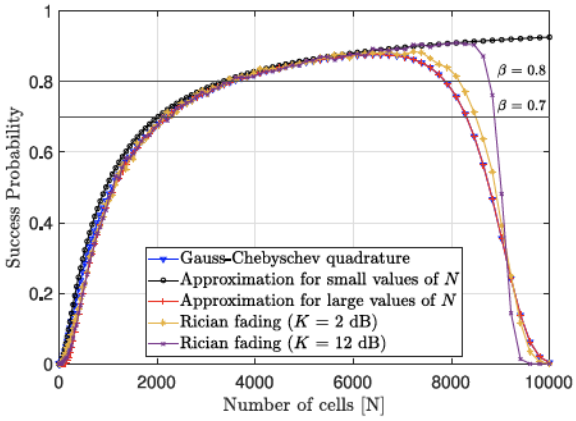

Fig. 2. Observing the behavior of $P_{suc}(N)$ from (11) for different values of N. We see that $P_{suc}(N)$ is an increasing function for smaller values of N and is a decreasing function for larger values of N. This aligns with Lemma 2 which describes the behavior of $f(N)$ for different ranges of N. Also, we simulate $P_{suc}(N)$ with Rician fading [15] between the EDs and the GW for a LoS channel. We observe that $P_{suc}(N)$ with Rician fading has a similar behavior to $P_{suc}(N)$ with Rayleigh fading from (11).

TABLE I
LPWAN Parameters Used for Simulations

Parameter	Notation	Value
ED density	λ_{ED}	10×10^{-6} devices/m^2
Probability of transmission	p	0.5
Transmit power	P	19 dBm
AWGN power spectral density	N_0	-174 dBm/Hz
Coverage area	A	$0 - 100$ km^2
LPWAN bandwidth	W	500 kHz
Carrier Frequency	f_c	915 MHz
Pathloss exponent	α	3
Target bit-rate	r	1500 bps
Success probability constraint	β	80%

Example 1: Consider an LPWAN system with parameters as described in Table I. We can compute F, G and H accordingly. For these parameters, if we consider a success probability threshold of $\beta = 0.8$, the minimum number of cells that satisfies the success probability constraint is, $N^{\star} = 3600$. Similarly, for $\beta = 0.7$ the minimum number of cells that satisfies the constraint is $N^{\star} = 2209$.

For the set of considered parameters, in Fig. 2, it can be observed that the approximation for small N (where we assume $2^{NG} \approx 1 + NG\log 2$) follows the original graph (with Gauss-Chebyshev quadrature) quite well when $N < 2000$. After that, when $N > 2000$, the approximation for large N (where we assume $2^{NG} >> 1$) works better.

V. Numerical Simulations and Discussion

In this section, we simulate the LPWAN system and validate the analytical results obtained in the previous sections. We consider a constant carrier frequency $f_c = 915$ MHz and a constant ED density of $\lambda_{ED} = 10 \times 10^{-6}$ devices/km^2. The parameters for the LPWAN system listed in Table I are sourced from studies related to multi-cell LoRa, including works by [9], [10], [11]. Now, first we investigate the effects of coverage area, number of cells, and observe the effect of active device density on success probability. Next, we explore the trend of optimal number of cells that ensures the guarantee of a minimum success probability. Finally, we

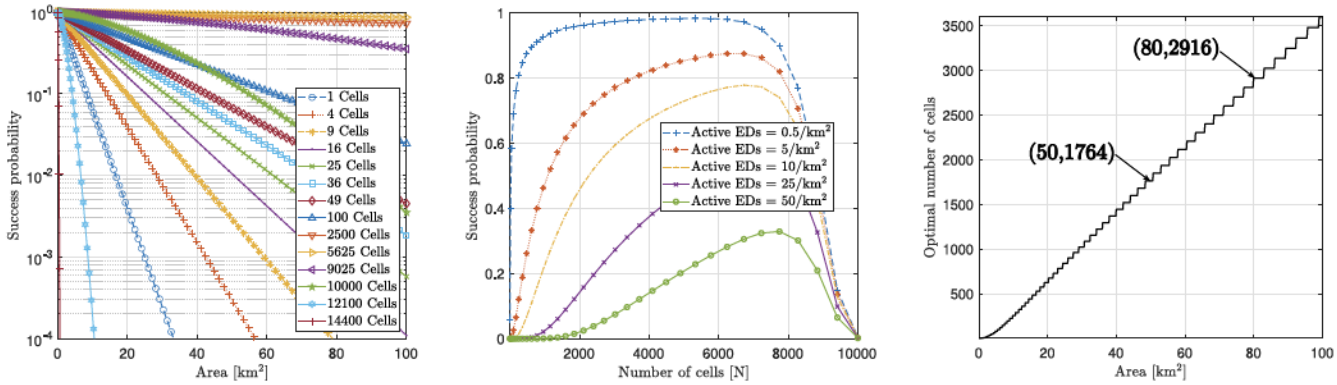

(a) Success probability of an ED at the cell edge in a multi-cell LPWAN for varying A. Note that $P_{suc}(N)$ decreases as A increases. Since the distance between the ED and the GW increases as A increases, the SINR at the GW decreases, which decreases $P_{suc}(N)$.

(b) Success probability of an ED at the cell edge in a multi-cell LPWAN for $A = 100$ km^2. Here, we vary the active device density λ_{AED} for a constant total bandwidth W. We observe that $P_{suc}(N)$ peaks at smaller values of N for less dense networks.

(c) Optimal number of cells for varying A and overall bandwidth $W = 500$ kHz. We observe that the optimal number of cells increases with coverage area A. Since the total number of interferers increase with A, we need more cells to achieve the constraint β.

Fig. 3. Illustrations of LPWAN scheme performance under different conditions.

conduct an experiment to compare the performance of our proposed scheme against LoRa [9].

Effect of coverage area: First, we examine the success probability of a multi-cell LPWAN for varying coverage area A using (11). The results are shown in Fig. 3(a) for different number of cells. We see that the success probability decreases as the overall coverage area A increases. We also observe that for a given area A, as the number of cells increases, the success probability first increases and then eventually starts to decrease, validating Lemma 2. This indicates that having an infinite number of cells does not necessarily enhance the success probability of transmission.

Effect of active ED density: Next, we analyze the impact of active device density on the success probability of a multi-cell LPWAN using (11). The results are shown in Fig. 3(b). We see that as the number of active devices decreases, the success probability increases. The interference power tends to be lower in a less dense network, assuming the same number of cells. This is also consistent with (4), where we see that the success probability of a less dense network will be higher.

Optimal number of cells: Now we compute the optimal number of cells in a multi-cell LPWAN using (12) for varying area A. The results are illustrated in Fig. 3(c), where we observe that $N^\star$ increases with A as we need more cells to cover a large area of active EDs. For example, the optimal number of cells for an area $A = 50$ km^2 is $N^\star = 1764$, whereas for $A = 80$ km^2, the value of $N^\star$ needs to be as large as 2916. Returning to (11), we know that F and H are increasing functions of A as $A = d^2$. For a constant N, this implies that $P_{suc}(N)$ decreases as A increases. Consequently, to meet the success probability (β) constraint, it is necessary to increase N. This interpretation aligns with the observations in Fig. 3(c).

Comparison of our proposed scheme with LoRa [9]: We conduct an experiment to compare our proposed method with LoRa [9]. We compare 36-cell and 100-cell LPWANs based on our scheme against corresponding LoRa networks with a deterministic GW configuration, unlike the random GW configurations in multi-cell LoRa [9], [11]. LoRa-specific parameters are obtained from [9], while other parameters are as mentioned in Table I. Using Monte-Carlo simulations, we generate multiple active device realizations and calculate SINR relative to the GW with the strongest signal, considering all EDs with the same spreading factors (SFs) as interferers. The success probability is determined based on SNR and Signal-to-Interference Ratio (SIR) constraints imposed by LoRa. The results, shown in Fig. 4, demonstrate that our scheme outperforms LoRa across all choices of A due to the mitigation of inter-cell interference through orthogonal frequency allocation.

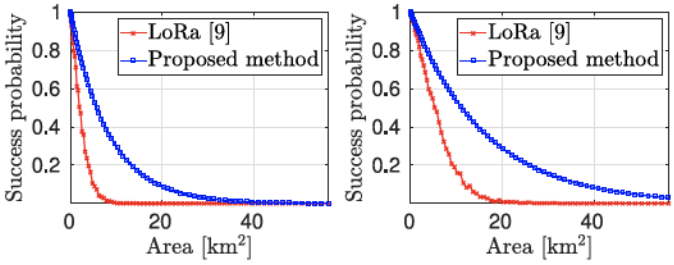

(a) 36 cell comparison

(b) 100 cell comparison

Fig. 4. A comparison of LoRa and our proposed scheme for LPWAN. A total bandwidth of $W = 125$ kHz is allocated for our scheme, whereas for LoRa, a bandwidth of 125 kHz is allocated per channel, and each LoRa GW has 4 spreading factors. We observe that our proposed scheme has a higher success probability with an overall bandwidth of $W = 125$ kHz against LoRa where 125 kHz is allocated per channel for the same area. Both the schemes have a device density of $\lambda_{ED} = 10 \times 10^{-6}$devices/m^2.

VI. Conclusion

In this letter, we explored the impact of small cells in LPWANs and designed a novel communication scheme that mitigates inter-cell interference. We conducted a mathematical analysis of intra-cell interference using stochastic geometry, resulting in a closed-form expression for the success probability of an ED at the cell edge. Utilizing this analysis, we computed the optimal number of cells that guarantee a minimum success probability required to cover an overall deployment region for IoT devices. Our results revealed the advantages of employing small cells with our scheme in the context of dense ED deployment within an LPWAN, showcasing superior performance compared to multi-cell LoRa.

APPENDIX A
PROOF FOR LEMMA 1

The MGF of the intra-cell interference is

$$\mathcal{L}_{\mathcal{I}_{cell}}(s) = \mathbb{E}_{\Phi_{AED},g_i}[\exp(-s\mathcal{I}_{cell})] = \mathbb{E}_{\Phi_{AED},g_i}\left[\prod_{i\in\Phi_{AED}} \exp\Big(-s\rho\ell(d_i)|g_i|^2\Big)\right]. \quad (13)$$

where $\mathcal{I}_{cell} = \sum_{i\in\Phi_{AED}} \rho\ell(d_i)|g_i|^2$. Now, the HPPP Φ_{AED} and the channel gain g_i are independent, therefore, the expectation terms can be split separately. Thus,

$$\mathcal{L}_{\mathcal{I}_{cell}}(s) = \mathbb{E}_{\Phi_{AED}}\left[\prod_{i\in\Phi_{AED}} \mathbb{E}_{g_i}\Big[\exp\Big(-s\rho\ell(d_i)|g_i|^2\Big)\Big]\right].$$

Now, we assume $f_{|g_i|^2}(x) = e^{-x}$ for Rayleigh fading, therefore, we can write [10],

$$\mathcal{L}_{\mathcal{I}_{cell}}(s) = \mathbb{E}_{\Phi_{AED}}\left[\prod_{i\in\Phi_{AED}} \frac{1}{1+s\rho\ell(d_i)}\right]. \quad (14)$$

Next, using the PGFL properly of HPPP [16, p. 235, A. 3], *i.e.*, $\mathbb{E}[\prod_{k\in\Phi} f(\mathbf{x_k})] = \exp(-\lambda\int_{\mathbb{R}^2}(1-f(\mathbf{x}))d\mathbf{x})$ and converting Cartesian to polar coordinates (14) can be simplified as

$$\mathcal{L}_{\mathcal{I}_{cell}}(s) = \exp\left(-p\lambda_{ED}\int_0^{2\pi}\int_0^R 1 - \frac{1}{1+s\rho\ell(x)}xdx\right) = \exp\left(-2\pi p\lambda_{ED}\int_0^R \frac{s\rho\kappa x^{-\alpha}}{1+s\rho\kappa x^{-\alpha}}xdx\right),$$

since $\ell(x) = \kappa x^{-\alpha}$.

APPENDIX B
PROOF FOR LEMMA 2

With the success probability of an N-cell LPWAN expressed as $P_{suc}(N) = e^{f(N)}$, from (11),

$$f(N) = -\frac{F\left(2^{NG}-1\right)}{N^{\frac{\alpha}{2}+1}} - \frac{H}{N}\sum_{k=1}^{n}\frac{c_k\sqrt{1-\psi_k^2}\left(2^{NG}-1\right)}{2^{NG}-1+c_k^{\alpha}}.$$

For small N, we have $2^{NG} \approx 1 + NG\log 2$, thus,

$$f(N) = -\frac{FG\log 2}{N^{\frac{\alpha}{2}}} - HG\log 2\sum_{k=1}^{n}\frac{c_k\sqrt{1-\psi_k^2}}{NG\log 2 + c_k^{\alpha}}. \quad (15)$$

Now, we can find the first derivative of $f(N)$ as

$$\frac{df(N)}{dN} = \frac{\alpha FG\log 2}{2N^{\frac{\alpha}{2}+1}} + H(G\log 2)^2\sum_{k=1}^{n}\frac{c_k\sqrt{1-\psi_k^2}}{\left(NG\log 2 + c_k^{\alpha}\right)^2}.$$

Since $F, G > 0$, $\frac{df(N)}{dN} > 0$. Hence, $f(N)$ is an increasing function for small N. Next, for large N, we have $2^{NG} >> 1$. Also $c_k^{\alpha} \leq 1$. Thus, $f(N)$ can be approximated as

$$f(N) = -\frac{F2^{NG}}{N^{\frac{\alpha}{2}+1}} - \frac{H}{N}\sum_{k=1}^{n} c_k\sqrt{1-\psi_k^2}, \text{ therefore, we have}$$

$$\frac{df(N)}{dN} = -\frac{F2^{NG}}{N^{\frac{\alpha}{2}+1}}\left[G\log 2 - \frac{\frac{\alpha}{2}+1}{N}\right] + \frac{H}{N^2}\sum_{k=1}^{n}\delta_k, \quad (16)$$

where $\delta_k = c_k\sqrt{1-\psi_k^2}$ for $k = 1, 2, \ldots, n$. Since $\psi_k \in [-1, 1]$, $c_k \in [0, 1]$, we have $0 \leq \delta_k \leq 1$. Now, $H = \frac{p\lambda_{ED}(\pi d)^2}{2n}$, this derivative can be upper bounded by

$$\frac{df(N)}{dN} \leq -\frac{F2^{NG}}{N^{\frac{\alpha}{2}+1}}\left[G\log 2 - \frac{\frac{\alpha}{2}+1}{N}\right] + \frac{p\lambda_{ED}(\pi d)^2}{2N^2}, = \frac{-F2^{NG+1}\left[G\log 2 - \frac{\frac{\alpha}{2}+1}{N}\right] + p\lambda_{ED}(\pi d)^2 N^{\frac{\alpha}{2}-1}}{2N^{\frac{\alpha}{2}+1}}$$

Now, we assume that N is large enough so that $N > \frac{\frac{\alpha}{2}+1}{G\log 2}$, therefore, $[G\log 2 - \frac{\frac{\alpha}{2}+1}{N}] > 0$. Moreover, we can find such a value for N which is large enough so that term 2^{NG+1} dominates over the terms $N^{\frac{\alpha}{2}-1}$. At this point, $\frac{df(N)}{dN} < 0$, which indicates that $f(N)$ is a decreasing function for large values of N, and concludes the proof.

Remark 1: Usually, N does not have to be very large to observe the decreasing property of $f(N)$. For instance, with the parameters in Table I, $\frac{df(N)}{dN} = -3.1\times10^{-4}$, when $N = 8100$. Thus, $f(N)$ is a decreasing function even for $N = 8100$ and remains so for larger values, as shown in Fig. 2.

REFERENCES

[1] (Ericsson, Stockholm, Sweden). *IoT Connections Outlook*. (2022). [Online]. Available: https://www.ericsson.com/en/reports-and-papers/mobility-report/dataforecasts/iot-connections-outlook

[2] Y. Zhang, D. J. Love, J. V. Krogmeier, C. R. Anderson, R. W. Heath, and D. R. Buckmaster, "Challenges and opportunities of future rural wireless communications," *IEEE Commun. Mag.*, vol. 59, no. 12, pp. 16–22, Dec. 2021.

[3] *Clemson Research Finds Using Soil Moisture Sensors Can Increase Farmers' Net Income: Clemson News*, Clemson Univ., Upstate South Carolina, SC, USA, 2021.

[4] "Growficient sensor." Growficient. Accessed: Apr. 6, 2024. [Online]. Available: https://www.growficient.com/en/sensor-2/

[5] K. Mekki, E. Bajic, F. Chaxel, and F. Meyer, "A comparative study of LPWAN technologies for large-scale IoT deployment," *ICT Exp.*, vol. 5, no. 1, pp. 1–7, 2019.

[6] F. Adelantado, X. Vilajosana, P. Tuset-Peiro, B. Martinez, J. Melia-Segui, and T. Watteyne, "Understanding the limits of LoRaWAN," *IEEE Commun. Mag.*, vol. 55, no. 9, pp. 34–40, Sep. 2017.

[7] "What is Sigfox." Sigfox. Accessed: May 24, 2024. [Online]. Available: https://www.sigfox.com/what-is-sigfox/

[8] S. Popli, R. K. Jha, and S. Jain, "A survey on energy efficient narrowband Internet of Things (NBIoT): Architecture, application and challenges," *IEEE Access*, vol. 7, pp. 16739–16776, 2019.

[9] L. Beltramelli, A. Mahmood, M. Gidlund, P. Österberg, and U. Jennehag, "Interference modelling in a multi-cell LoRa system," in *Proc. 14th Int. Conf. Wireless Mobile Comput., Netw. Commun. (WiMob)*, 2018, pp. 1–8.

[10] Z. Qin, Y. Liu, G. Y. Li, and J. A. McCann, "Modelling and analysis of low-power wide-area networks," in *Proc. IEEE Int. Conf. Commun. (ICC)*, 2017, pp. 1–7.

[11] O. Georgiou, C. Psomas, and I. Krikidis, "Coverage scalability analysis of multi-cell LoRa networks," in *Proc. IEEE Int. Conf. Commun. (ICC)*, 2020, pp. 1–7.

[12] M. Haenggi, *Stochastic Geometry for Wireless Networks*. Cambridge, U.K.: Cambridge Univ. Press, 2012.

[13] R. B. Sorensen, N. Razmi, J. J. Nielsen, and P. Popovski, "Analysis of LoRaWAN uplink with multiple demodulating paths and capture effect," in *Proc. IEEE Int. Conf. Commun. (ICC)*, 2019, pp. 1–6.

[14] F. B. Hildebrand, *Introduction to Numerical Analysis*. North Chelmsford, MA, USA: Courier Corp., 1987.

[15] S. Zhu et al., "Probability distribution of Rician K-factor in urban, suburban and rural areas using real-world captured data," *IEEE Trans. Antennas Propag.*, vol. 62, no. 7, pp. 3835–3839, Jul. 2014.

[16] M. Haenggi and R. K. Ganti, *Interference in Large Wireless Networks*. Hanover, MA, USA: Now Publ., 2009.